Effect of mischmetal concentration and superheating on the microstructure and tensile properties A319.1: Role of Fe content

H.W. Doty [a], E. Samuel [b], A.M. Samuel [b], E. Elsharkawi [c], V. Songmene [d], F.H. Samuel [b,*]

[a] *Materials Technology, General Motors Global Technology Center, Warren, MI, 48092, USA*
[b] *Université du Québec à Chicoutimi, Saguenay, QC, Canada*
[c] *Saint Mary's University, Halifax, NS, Canada*
[d] *Department of Mechanical Engineering, École de Technologie supérieure, QC, Canada*

ABSTRACT

The aim of this research is to study the effect of certain metallurgical parameters such as the addition of a mixture of rare earths (mischmetal) and superheating on the microstructure and tensile properties of the Al–Si–Cu alloy A319.2 containing 0.4%, 0.8% and 1.2% iron used in the automotive industry. The mischmetal (MM) precipitates in the form of platelets like the β-Al_5FeSi leading to a marked refinement in eutectic Si particles at 5% MM. In addition, α- $Al_{15}(Fe,Mn)_3Si_2$. segregated particles and mischmetal-bound intermetallics persist in the microstructure even after T6 heat treatment. The tensile properties of 0.8% iron alloys deteriorate when the mischmetal concentration and superheat temperature increase, although the silicon phase undergoes significant changes. Alloys with a high iron concentration (1.2% Fe) showed a slight decrease in the length of the β-Al_5FeSi phase platelets and of the mischmetal compared to alloys with 0.4% and 0.8% Fe when the concentration of mischmetal increases to 5% and when the superheating temperature reaches 950 °C. This observation explains the increase in the % elongation to fracture of the 1.2% Fe-5% mischmetal alloy cast directly from 750 °C or after superheating at 950 °C, followed by in-furnace cooling to 750 °C. The ultimate tensile strength and yield strength degrade with mischmetal, but improve slightly with superheating; only for the 1.2% Fe-0% mischmetal alloy, its yield strength decreases once superheated to 950 °C.

1. Introduction

In the last decade, light metals and in particular, aluminum alloys, have been used in the automotive industry to make cars lighter. However, this alloy must have good strength and machinability [1]. During the solidification process of these alloys, several phases are formed: pre-eutectic, co-eutectic and post-eutectic. Among the phases that make up one of the most popular alloys, A319 (hypo-eutectic), the β-Fe phase (Al_5FeSi) is the most harmful as it significantly decreases ductility [2–4]. The most reliable values of the eutectic point from the Al–Si diagram are 577 °C and 11.8% silicon (by weight), which corresponds to an atomic percentage of silicon of 11.2–11.4. Their dependence between temperature and solubility has been determined by several authors [5–7] in using different methods. Under equilibrium conditions, the phases present in the solid state show a low solubility of silicon in aluminum when a small quantity of iron is added. Under non-equilibrium conditions, four phases can be encountered simultaneously: Al, Si, α- and β-AlFeSi)

[8,9]. In the Al–Si–Cu–Fe alloys, however, formation of Al_7Cu_2Fe phase was reported to form containing an average of 60.42 at. %Al, 27.73 at. % Cu, 8.83 at. %Fe using WDS analysis [10]. Fig. 1 shows the formation of AlCuFe phase at the edges of β -AlFeSi platelet (Fig. 1a), whereas Fig. 1b and c depict the distribution of Cu and Fe in Al_7Cu_2Fe.

Intermetallics are generally divided into three morphologies: crystal polygonals, Chinese script and thin plates. Equilibrium phase diagrams of diluted Al–Fe–Si alloys, include the phases Θ-AlFeSi (monoclinic), α-Al_8Fe_2Si (hexagonal), β-Al_5FeSi (monoclinic) and the α-phase whose chemical composition is $Al_{12}Fe_3Si_2$ (30.7% Fe, 10.2% Si). These phases dominate during slow solidification, so that metastable phases like Al_6Fe (orthorhombic) and α-$Al_{20}Fe_5Si_2$ (cubic) are precipitated during quenching or rapid solidification. In several alloys, commercial aluminum products contain manganese or chromium as an impurity. It is concluded that the β-phase solidification during liquid-solid (pre-eutectic) and during the formation of the eutectic (co-eutectic), when the iron concentration exceeds 0.7% [11–13].
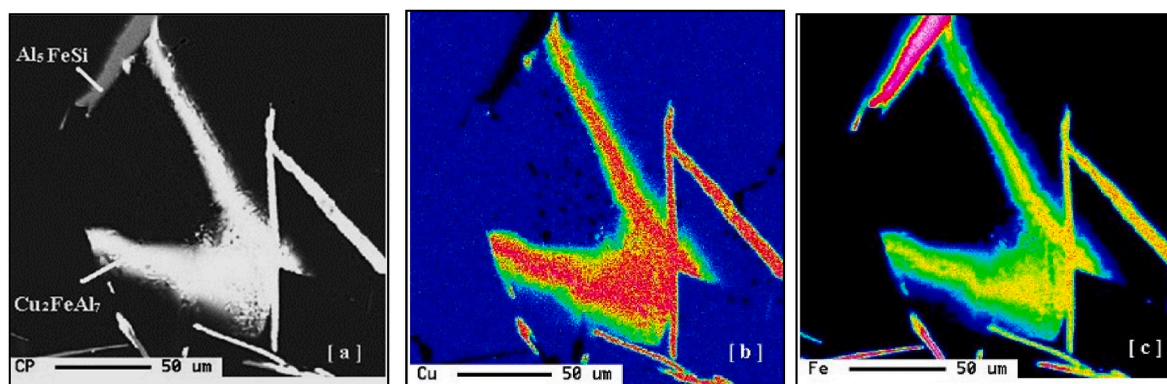
Fig. 1. Distribution of Cu and Fe elements in the Al7Cu2Fe: (a) Backscattered electron image, (b,c) display the distribution of Cu and Fr, respectively in (a).
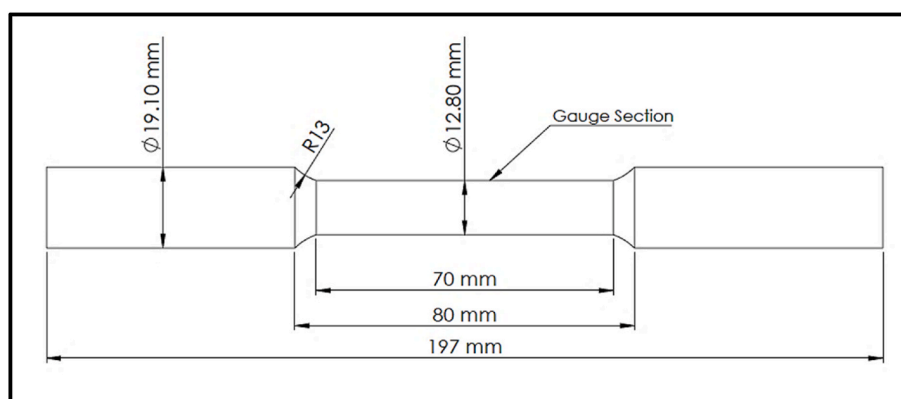

Fig. 2a. Geometry of the standard tensile test bar obtained from ASTM B-108 permanent mold.
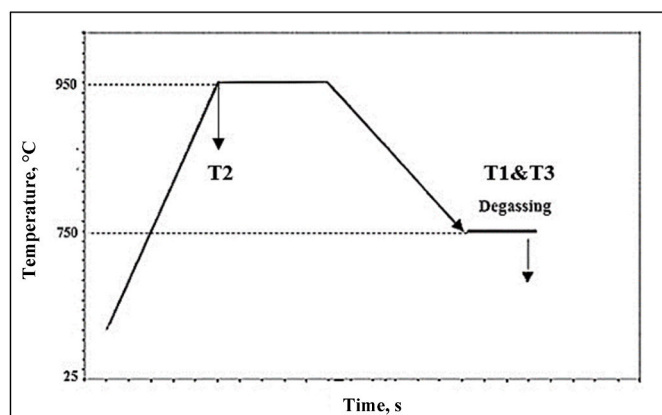

Fig. 2b. Schematic diagram illustrating the different pouring temperatures: T1 = pouring directly from 750 °C, T2 = pouring directly from 950 °C, T3 = pouring directly from 750 °C, following superheating at 950 °C for 15 min. Schematic diagram illustrating the dimensions and shape of the graphite mold

Increasing the melting temperature has been proposed to eliminate the β-AlFeSi (which is harmful to the mechanical properties of aluminum alloys). Superheating transforms the β-AlFeSi phase into Chinese script. Superheating coupled with rapid solidification reduce the interdendritic space, the size of the constituents of the eutectic and Fe-containing phases as well as the grain size, despite the increase in the real time of solidification [14,15]. In addition, aluminum alloys contain a nucleation catalyst which act at the zero-undercooling point and when the superheating exceeds 500 °C, the size and possibly the number of

nucleation particles are reduced, but do not eliminate them completely.

A lot of research work [16,17] has been carried out concerning the use of rare earths metals as a grain refining agent for pure aluminum and its alloys or as modifying agents in Al–Si foundry alloys. Rare earths metals are widely used as modifying agents in Al–Si alloys but in different quantities ranging from 0.02% by weight to 3%. As a grain refining agent, the effect of rare earths metals (individually or in the form of mischmetal) is less documented. But some publications were the subject of the effects of the latter on the dendrite arm spacings (SDAS) of the α-Al phase of the microstructure of foundry alloys. This SDAS is very important for the properties of forged aluminum alloys and is also more important than the grain size of foundry alloys [18].

The effect of mischmetal and cerium on the hot work hardening and mechanical properties of wrought Al–Mg–Si alloys has been studied by several researchers [19]. The experimental results obtained show that the hot plasticity of Al–Mg–Si alloys may be increased and the hardness and strength can be slightly improved by adding more than 0.1% by weight of RE [20]. Below this value, certain properties may be deteriorated. Improving the machinability and surface finish of certain aluminum alloys is also obtained by adding rare earths. Other works that focused on the effect of rare earths on electrical conductivity and mechanical properties showed that adding 0.6% by weight of lanthanum not only increased electrical conductivity, but apparently produced an improvement in elongation and tensile strength. The optimal quantities of rare earth metals or types of rare earths to add remain to be determined. In fact, this leads to the introduction of impurities into the rare earth metals or damage the properties of the alloy.

Rare earth metals, known as lanthanides, belong to a group of 15 elements in group III of the periodic table of chemical elements. A mixture of lanthanides in metallic form, called "mischmetal", is used as a modifying agent of the phase of eutectic silicon in the present work of

Table 1
Chemical composition of the used mischmetal (wt.%).

	Ce	La	Pr	Nd	Al
Mischmetal (MM)	10	7	1	1	81

Table 2
Chemical compositions of alloys studied in the present work (wt%).

Alloy codes	Si	Fe	Cu	Mn	Mg	Ti	Ce[a]	La[a]
B0MT1[a] (0 % MM)	6.24	0.38	3.65	0.09	0.07	0.14	–	–
B0MT2[b] (0 % MM)	6.25	0.43	3.52	0.1	0.08	0.14	–	–
B1MT1 (1 % MM)	6.16	0.39	3.61	0.1	0.07	0.14	0.09	0.07
B1MT2 (1 % MM)	6.25	0.44	3.6	0.1	0.08	0.14	0.09	0.07
B3MT1 (3 % MM)	6.12	0.44	3.57	0.09	0.07	0.14	0.28	0.21
B3MT2 (3 % MM)	6.17	0.41	3.58	0.09	0.07	0.14	0.28	0.21
B5MT1 (5 % MM)	6.17	0.43	3.59	0.1	0.07	9.13	0.47	0.34
B5MT2 (5 % MM)	6.15	0.48	3.59	0.09	0.07	0.14	0.47	0.34
B1F0MT1 (0 % MM)	6.12	0.84	3.48	0.09	0.04	0.14	–	–
B1F0MT2 (0 % MM)	6.62	0.81	3.5	0.12	0.03	0.15	–	–
B1F1MT1 (1 % MM)	6.08	0.85	3.49	0.12	0.05	0.20	0.09	0.07
B1F1MT2 (1 % MM)	6.32	0.85	3.45	0.12	0.03	0.15	0.09	0.07
B1F3MT1 (3 % MM)	5.79	0.85	3.3	0.12	0.03	0.23	0.28	0.21
B1F3MT2 (3 % MM)	6.27	0.84	3.41	0.12	0.03	0.14	0.28	0.21
B1F5MT1 (5 % MM)	5.71	0.84	3.25	0.11	0.03	0.28	0.47	0.34
B1F5MT2 (5 % MM)	6.23	0.85	3.41	0.12	0.03	0.15	0.47	0.34

[a] T1 = 750 °C.
[b] T2 = 950 °C.

research. The composition varies depending on the source of the original mineral. The main constituents are cerium (50%–55%), lanthanum (23%–27%) and neodymium (10%). The mischmetal used in this research work contains 80% aluminum and the rest is made up of rare earths. The mischmetal added to magnesium alloys improves creep resistance while in aluminum alloys it promotes grain refinement and increases fluidity [21,22].

Colomobo et al. [23,24] investigated the effect of addition of Er and Zr on the microstructure and tensile properties of Al–Si–Mg cast alloys. Their funding showed the effectiveness of using Er in modifying the Si eutectic resulting in a similar behavior of Sr in the as-cast condition. Also, increasing the concentrations of Er and Zr, the alloy hardness in the peak aging as well as following prolonged exposure to high temperatures was higher than that of the base alloy. The work of Barkov et al. [25,26] indicates that Er and Zr increase the artificial aging at temperatures as high as 210 °C, improve the yield stress at elevated temperatures coupled with reducing the tendency to soften during annealing due to dispersoids formed during homogenization. The effect of Eu (Europium) element on eutectic Si in Al–7Si alloys was studied by Mao et al. [27]. The results indicate that the addition of Eu changes the morphology of eutectic Si from coarse plate-like to fine fibrous similar to the use of Sr, decreasing at the same time the eutectic nucleation temperature, which is caused by the poisoning of AlP particles by Eu.

The alloy studied in this project is the aluminum alloy A319 to which different amounts of a mixture of rare earth metals called "misch-metal" are added. These alloys undergo two different superheats; in this case, as

the molten metal was cast directly from two temperatures: T1 = 750 °C and T2 = 950 °C. The aim of the mechanical tests in the present project is to obtain property values which will be useable in calculations of the strength of materials or which will make it possible to assess the behaviour of a material in use. The mechanical properties of alloys depend on the SDAS, the level of modification of the eutectic silicon phase.

2. - Experimental methodology

2.1. Preparation of tensile specimens

The chemical composition of the alloys which is given in Table 1 are prepared using ingots of the base alloy A319. These alloys which are dried and cleaned are placed in a 28 kg silicon carbide crucible and melted at two temperatures, 750 °C and 950 °C. The molten metal was degassed by argon using a graphite impeller rotating at 150 rpm. The electric furnace is equipped with a baffle made of refractory product to prevent the formation of a vortex that can carry oxides into the liquid metal. The iron and mischmetal additions were made when the metal began to melt. All the castings were made in optimal conditions of humidity were about 15% and temperature of surroundings was ~22 °C. The grain refinement was achieved using Al-5 wt.% Ti-1 wt.% B master alloy to obtain a level of ~0.2 wt% Ti in the final alloys. The iron addition was done using Al-25 wt% Fe master alloy to achieve the required concentrations of 0.4%, 0.8% and 1.2% whereas mischmetal was used in the form of a mixture of La and Ce (as shown in Table 1). Three samplings for chemical analysis were taken and the chemical analysis was carried out using a Spectrolab -JrCCD Spark Analyzer. The average chemical compositions (three burns per alloy sample) are reported in Table 2.

The tensile bars were obtained by casting each alloy in the Stahl metal mold of type ASTM B-108 (Fig. 2a) preheated to 450 °C. Alloys containing a high level of iron have shown good fluidity when cast directly at the temperature of the 950 °C (Fig. 2b schematizes the casting conditions). Sound castings (Fig. 2c), could not be obtained due to their excessive fluidity. The work carried out on the thermal cycle shows that it is possible to cool the metal in the furnace from 950 °C to 750 °C, and then pour it at this temperature into the metallic mold. Indeed, the same properties are obtained with this thermal cycle as after direct casting at 950 °C. This method is necessary when it is a question of large quantities of liquid metal to be cast. Sound castings, as shown in Fig. 2d, were not obtained due to their excessive fluidity.

2.2. Thermal analysis

In order to obtain the solidification curves and to identify the possible reactions and their formation temperatures, thermal analysis was carried out. The molten metal of each composition was poured into a hot (600 °C) cylindrical graphite mold of 80 mm height and 60 mm diameter. A high sensitivity Type-K (chromel-alumel) thermocouple was attached to the centre of the graphite mold. The temperature-time data was collected using a high-speed data acquisition system. The solidification curves and their first derivative curves were plotted in order to identify the main reactions that would take place during solidification with their corresponding formation temperatures. Samples, 2.5 × 2.5 cm in cross-section, were machined from the central section of the graphite mold, and polished microstructural analysis- Fig. 2f.

2.3. T6 heat treatment

The improvement of the mechanical properties of A319 alloys is only possible with a solution treatment which is followed by quenching and then ageing (standard T6 thermal treatment). The solution and aging were carried out in a CFD-147 model forced-air electric furnace. The air circulation allows the temperature to be evenly distributed. The samples
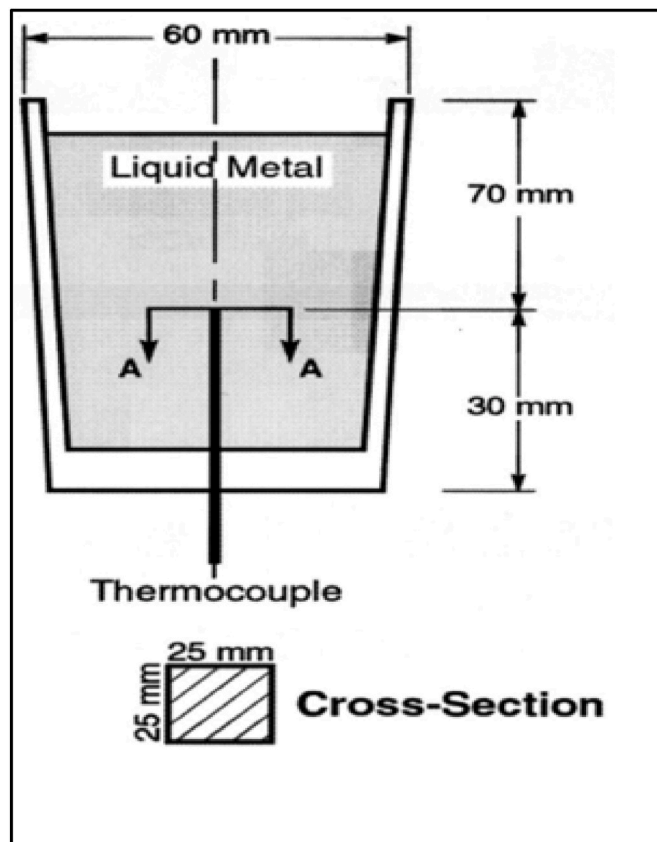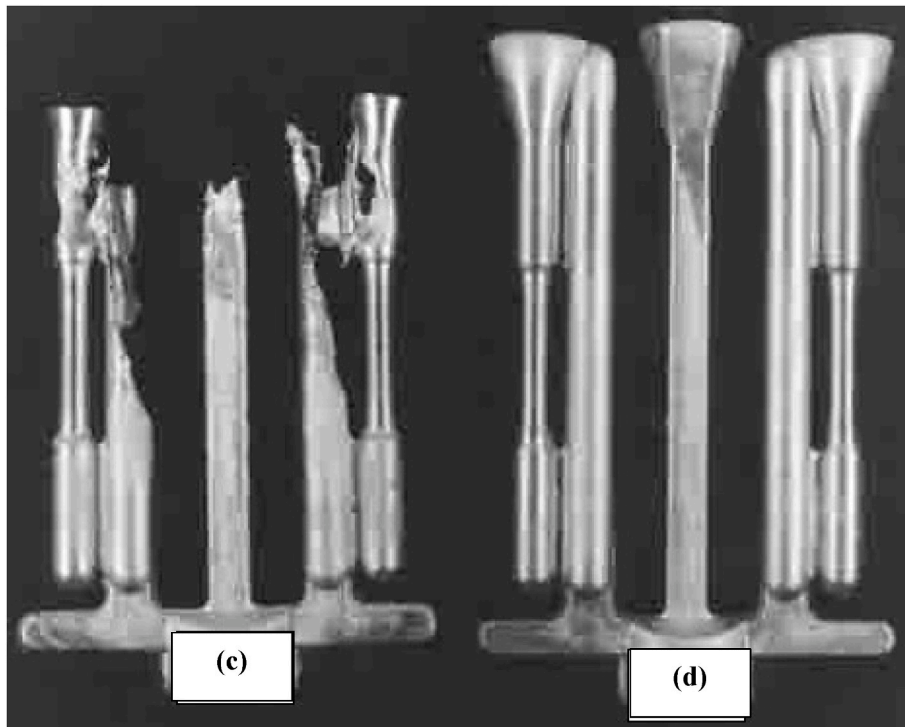
Fig. 2c and d. (c): casting obtained from 950 °C melt temperature, (d) casting obtained from 750 °C melt temperature- ASTM-B801 mold.

are placed in the furnace and the temperature is reduced to 500 °C over a period of 8 h. The solution was carried out at a temperature of 500 °C for 8 h to dissolve the aluminum-soluble phases such as the Al_2Cu and Mg_2Si phases and to prevent their melting. The solution is followed by a water quenching in a bath heated to 60 °C which makes it possible to maintain supersaturation of the dissolved phases and at the same time to reduce the stresses that may exist if the water is cold. The ageing treatment which lasts 5 h at 155 °C aims to precipitate the hardening phases (Mg_2Si, Al_2Cu, Q-$Al_5Mg_8Cu_2Si_6$) into a fine dispersed form [28–30].
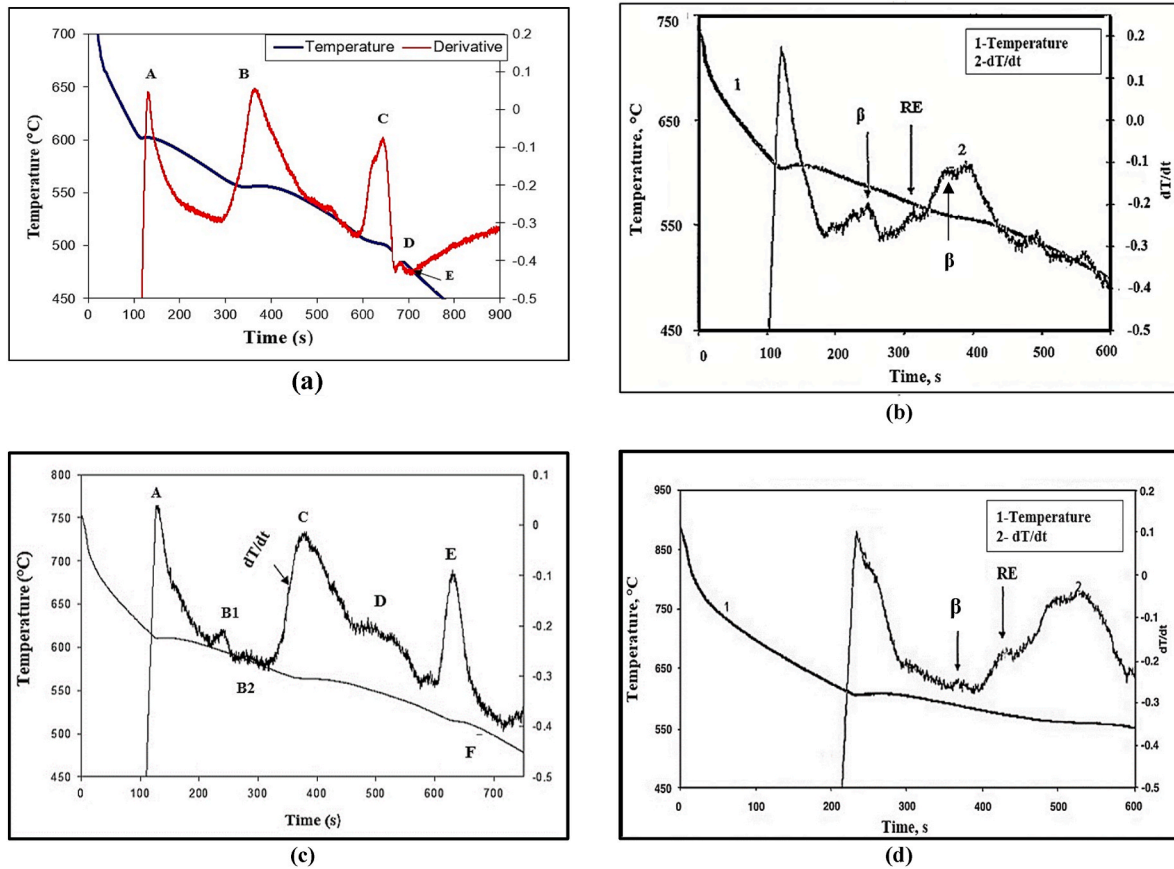
Fig. 3. Solidification curves and first derivatives obtained from:(a) as received A319.1 alloy-0.45%Fe, (b) A319.1 + 0.83 %Fe+5%MM (0.46 RE),(c) A319.1 + 1.2 % Fe+5%MM-poured from 750 °C, (d) A319.1 + 1.2 %Fe+5%MM-poured from 950 °C.

Table 3
Reactions Observed in A319 alloy containing 0.4% and 0.8%Fe at ∼ 0.8 °C/s.

Alloy	Peak	Temperature (°C)	Reaction
A319 G Fig. 3a	A	601.26	Development of α-Al dendrite network
	B	558.54	Al–Si eutectic reaction
	C	504.63	Al–Al$_2$Cu eutectic reaction
	D	487.63	Traces of Q-Al$_5$Cu$_2$Mg$_8$Si$_6$
	E	486.84	End of reaction
A319 G + 0.84%Fe+ 5%MM (Fig. 3b**)**	A	610.26	Development of α-Al dendrite network
	B1	595.33	⟶ Liq. β-Al$_5$FeSi phase
	B2	590.0	Solidification of RE phase(s)
	C	563.54	Al–Si eutectic reaction
	D	551.23	⟶ Liq. Al + Si + Al5FeSi reactions
	E	514.63	Al–Al$_2$Cu eutectic reaction
	F	491.63	End of solidification
A319 G + 1.2 %Fe+ 5%MM (Fig. 3c**)**	A	610.3	Development of α-Al dendrite network
	B1	605.5	⟶ Liq. β-Al$_5$FeSi phase
	B2	590.0	Solidification of RE phase(s)
	C	563.54	Al–Si eutectic reaction
	D	551.23	⟶ Liq. Al + Si + Al$_5$FeSi reactions
	E	510.63	Al–Al$_2$Cu eutectic reaction
	F	491.63	End of solidification
A319 M + 1.2%Fe+ 5%MM (Fig. 5a**)**	A	600	Development of α-Al dendrite network
	B	550.33	Al–Si eutectic reaction
	C	517.0	Al–Al$_2$Cu eutectic reaction

2.4. Tensile testing

The tensile bars were tested with an Instron machine at a constant speed of 0.5 mm/min (4×10^{-4}/s) at room temperature. The data acquisition system is connected to the servo-hydraulic MTS machine. Software transforms force into stress and elongation into deformation. Six to eight tests per alloy were performed to obtain the mean and standard deviation of the following parameters: yield strength (YS), ultimate tensile strength (UTS) and elongation percent (%EL).

2.5. Metallography

For the metallographic analysis, the sample was taken a few centimeters from the rupture zone. Part of the microstructure analysis was performed with the optical microscope, while another part including the fracture mode analysis was performed using a Hitachi SU-8000 field emission scanning electron microscope (FE-SEM), equipped with a secondary electron detector (SE), a backscatter electron detector (BSD) and Energy dispersive X-ray spectrometer (EDS).

3. Results and discussion

3.1. Thermal analysis

For the purpose of investigating the undercooling associated with the addition of Fe or Fe + RE, samples were not grain refined. Fig. 3 shows the solidification curves revealing two major observations - melts were not grain refined or modified with Sr. Table 3 shows the reactions observed in A319 alloy containing 0.4% and 0.8%Fe at ∼ 0.8 °C/s. Table 4 reveals solidification parameters of the present alloys-0.46%Fe.:

Table 4
Solidification parameters of the present alloys-0.46%Fe.

Alloy	Nucleation temperature T_{N1} (ºC)	Growth temperature T_{N2} (ºC)	Supercooling $\Delta T = T_{N1} - T_{N2}$ (ºC)	Interdendritic space DAS (μm)	Standard Deviation DAS (μm)	Beginning of solidification t_{TN1} (sec)	Beginning of growth t_{TN2} (sec)	Duration of nucleation t_{TN1}-t_{TN2} (sec)
B[a]0 MG[b]T1 (0%MM)	603	604	1	67.64	8	93.2	101.4	8.2
B0MGT2 (0%MM)	599	601	2	65.64	13	206.8	227	20.2
B1MGT1 (1%MM)	602	604	2	58.11	10	105.2	123.6	18.4
B1MGT2 (1%MM)	602	604	2	64.22	7	199	220.4	21.4
B3MGT1 (3%MM)	604	606	2	61.62	10	160.2	179.8	19.6
B3MGT2 (3%MM)	602	604	2	63.4	11	253.2	273.3	20.1
B5MGT1 (5%MM)	603	606	3	64.46	12	153.8	172.2	18.4
B5MGT2 (5%MM)	602	604	2	67.15	13	197.4	226.2	28.8
B0MM[c]T1 (0%MM)	599	599	0	18.27	3	1.6	1.6	–
B0MMT2 (0%MM)	593	594	1	15.77	3	3.2	3.8	0.6
B1MMT1 (1%MM)	595	597	2	16.43	3	2.1	3.1	1
B1MMT2 (1%MM)	596	597	1	15.61	3	2.9	3.3	0.4
B3MMT1 (3%MM)	601	601	0	15.41	2	1.7	1.7	–
B3MMT2 (3%MM)	597	597	0	13.4	1	2.9	2.9	–
B5MMT1 (5%MM)	600	601	1	14.93	3	1.7	2.1	0.4
B5MMT2 (5%MM)	597	598	1	12.59	1	2.9	3.7	0.8

[a] M = MM.
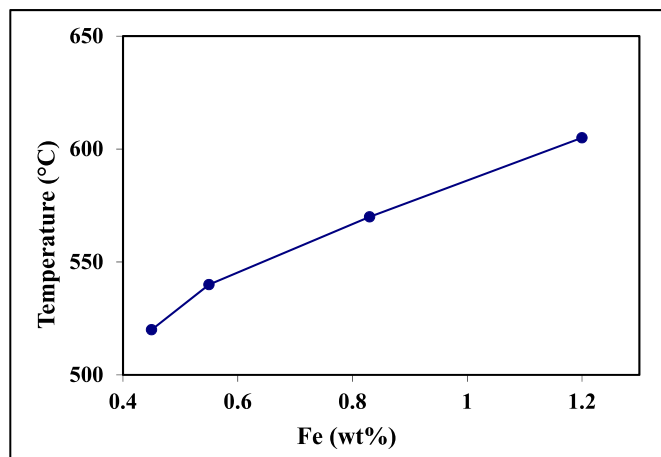[b] G = graphite.
[c] M = metallic.

Fig. 4. Fe content vs. β-phase formation temperature.

1. The addition of RE leads to increasing the undercooling, reaching 4 °C at 0.61% RE, through lowering the temperature of beginning of solidification.
2. Pouring directly from 750 °C without superheating is consistently one degree higher than 950 °C due to the presence of oxides that would assist in grain nucleation.
3. Explicit peak corresponding to precipitation of β-platelets could be observed at Fe content above 0.8%. Fe content versus β-phase formation temperature is shiown in Fig. 4.

4. There is a linear-relationship between the Fe% and the formation temperature of β-phase as displayed in Fig. 13 which is good confirmation of the data presented by Narayanan et al. [31] and Musmar et al. [32].
5. At high Fe content e.g., 0.57%, β-phase precipitates as pre-eutectic and co-eutectic as shown in Fig. 3b.
6. In the present work, RE-phase(s) precipitated at about 610 °C, in-dependent of the formation temperature of iron phases-Fig. 3b and 3c.
7. Pouring the liquid metal directly from 950 °C, Fig. 3d, has a marginal effect of the formation temperatures of β-, and Re -phases. However, the undercooling has been totally eliminated.
8. Application of high solidification rate (metallic mold-15-20μm dendrite arm spacing) resulted in elimination; most of details were exhibited using hot graphite mold (65–80 μm dendrite arm spacing) as shown in Fig. 5. In this case, only three peaks have been observed: α-Al, precipitation of Al–Si eutectic reaction, and precipitation of Al–Cu eutectic reaction, with complete elimination of α-Al undercooling.
9. Increasing the pouring temperature from 750 °C to 950 °C has no significant effect on the solidification curve obtained from 750 °C.

The characteristics of these intermetallic compounds are listed in Table 6. It is not possible to match of these peaks at the RE phase due to a lack of evidence. The new phases linked to mischmetal are observable on the solidification curves for two values of the iron concentration in this case 0.8% and 1.2%. Phase density RE, is calculated by subtracting the density of the β-phase measured for the 0 % alloy mischmetal to that of the 5%-mischmetal to significantly quantify the RE phase. The density of the latter increases with the iron concentration in cast alloys,
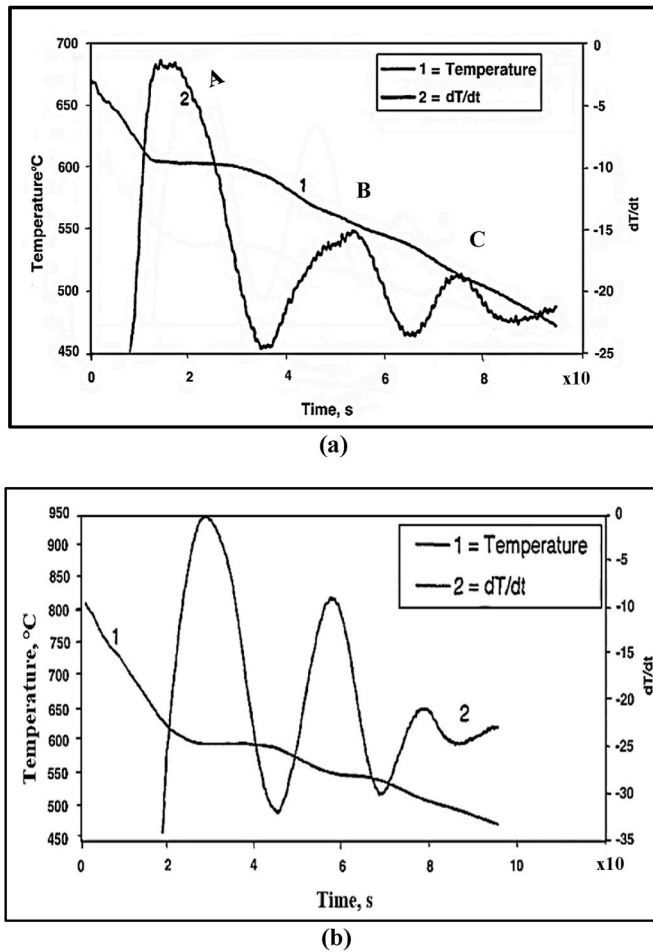
Fig. 5. Solidification curves and their first derivation obtained from 319 alloy samples cast in a metallic mold containing 1.2%Fe +%%RE: (a) poured from 750 °C, (b) poured directly from 950 °C.

Table 5
The formation temperatures of intermetallic phases with mischmetal (alloys were cast in graphite mold at T1 = 750 C and T2 = 950 C, 5% of misch, metals (MM).

Alloy	Phase	Temperature	Density P/mm²	Length μm	Width μm
0.4% Fe5% MM T1	Post-eutectic β / β and MM / MM	545 °C	113 / 46	β and MM μ = 95, σ = 132	β and MM μ = 4, σ = 2
0.4% Fe5% MM T2	Post-eutectic β / β and MM / MM	544 °C	141 / 111	β and MM μ = 81, σ = 64	β and MM μ = 3, σ = 2
0.8% Fe5% MM T1	Mischmetal MM1 / Pre-eutectic α / Pre-eutectic β Mischmetal MM2 / β and MM / MM	605 °C / 592 °C / 579 °C / 566 °C	0.04 / 314 / 118	β and MM μ = 81, σ = 121	β and MM μ = 3, σ = 3
0.8% Fe5% MM T2	Mischmetal MM1 / Pre-eutectic β Mischmetal MM2 / β and MM / MM	606 °C / 585 °C / 571 °C	298 / 69	β and MM μ = 85, σ = 45	β and MM μ = 4, σ = 2
1.2% Fe5% MM T1	Pre-eutectic β / Mischmetal MM2 / β and MM / MM	585 °C / 568 °C	824 / 422	β and MM μ = 91, σ = 84	β and MM μ = 4, σ = 1
1.2% Fe5% MM T2	Pre-eutectic β / β and MM / MM	585 °C	336 / 199	β and MM μ = 54, σ = 46	β and MM μ = 2, σ = 1

μ = average, σ-SD.

temperature 750 °C. The same phenomenon is observed when each alloy is cast at the superheating temperature 950 °C, except for the 0.8% iron 5% mischmetal containing alloy.

Due to the similarity in the brightness of MM or more precisely RE, it is difficult to distinguish between β-platelets and RE platelets. Thus, in Table 5, the dimensions and density were calculated for both. The new phases linked to mischmetal are observable on the cooling curves for two values of the iron concentration, in this case 0.8% and 1.2%. Phase density of RE precipitated phases (MM), is calculated by subtracting the density of the β-phase measured for the 0%- alloy mischmetal to that of the 5%-mischmetal alloy. The study was limited to 0%-mischmetal and 5%-mischmetal to significantly quantify the MM phase. The density of the latter increases with the iron concentration in cast alloys temperature Tl = 750 °C. The same phenomenon is observed when each alloy is cast at the superheating temperature T2 = 950 °C.

In 5% mischmetal containing alloys, the density of the α-Fe increases with the iron concentration, in alloys cast at temperature Tl unlike alloys at 0% of mischmetal. In this case, it can be considered that the iron or the phase which it is associated as a nucleation agent of α-phase, because the concentration of manganese is constant. However, when the alloys are superheated to T2 = 950 °C, the density of the latter decreases when the iron concentration increases. This shows that superheating destroys the germination agent of α-phase when the iron level increases to 0.8% or more as shown in Fig. 6.

3.2. Microstructural characterization

In this section, the main microstructural features will be reviewed in the as-cast condition. All samples were not grain refined or modified with Sr and poured from 750 °C. Fig. 7a shows the microstructure of the base alloy solidified at the rate of ∼0.8 °C/s (graphite mold) revealing the precipitation of Al₂Cu phase particles on the wide surface of the precipitated β-platelets. Since the formation temperature of β-phase is low ∼505 °C, their growth rates are limited. The details of Al₂Cu are illustrated in Fig. 7b where a network can be seen precipitated on the surfaces unmodified Si particles and of α-Fe particles. The black arrow in the inset point to fine Si particles representing the end of solidification.

The effect of increasing the Fe content on the dimensions of β-platelets is displayed in Fig. 8a where the length of the platelets could reach ∼500–600 μm which could block the movement of the liquid metal leading to the formation of large porosities (Fig. 8b) which could overcome to some extent by pouring the molten metal from ∼950 °C or the use of Sr modification or both as demonstrated in Fig. 8c. In contrast to β-platelets, precipitation of α-Fe does not lead to porosity formation as depicted in Fig. 8d.

Another point to be considered is the precipitation of RE. To emphasize on this point, the microstructure of the alloy containing 0.46%-5%MM has been examined as exhibited in Fig. 9a where thin curved platelets (<0.5 μm, almost 1/10th of β-platelets depicted in Fig. 8b) can easily be soon. The curvature of these platelets is caused by the movement of the liquid metal excreting pressure on the surfaces of the RE platelets. The morphology and density of RE-based intermetallics are clear in Fig. 9b, a backscattered electron image of 9a. High magnification of Fig. 9a is presented in Fig. 9c revealing the precipitation of eutectic Si particles on the surfaces of RE phase precipitated particles leading to gradual refinement of the Si particles as listed in Table 6. The

Table 6

Analysis of silicon particle characteristics of alloys after T6 heat treatment.

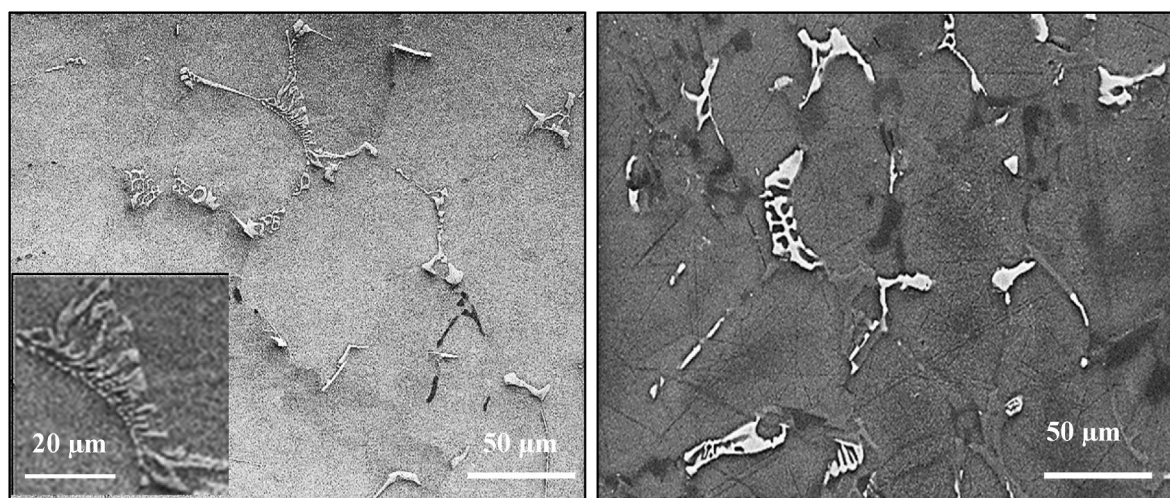| Alloy	Average Surface Area (%)	Average Surface Area of each particle	Length of each particle	The length/width ratio for each particle	Particles Density /mm²
0.4%Fe −0 MM-T1	μ = 4.9	μ = 9.5	μ = 5.5	μ = 23	5500
	σ = 0.7	σ = 11.1	σ = 4.6	σ = 1.2	
0.4%Fe-0%MM-T3	μ = 4.0	μ = 5.9	μ = 3.8	μ = 1.9	6850
	σ = 3.5	σ = 7.3	σ = 2.9	σ = 0.8	
0.4%Fe-5%MM, T1	μ = 3.5	μ = 8.3	μ = 5.0	μ = 2.1	4354
	σ = 0.5	σ = 4.9	σ = 3.2	σ = 0.9	
0.4%Fe-5%MM, T3	μ = 3.5	μ = 7.3	μ = 4.3	μ = 2.0	4746
	σ = 2.6	σ = 2.9	σ = 3.6	σ = 0.8	
0.8%Fe-0%MM, T1	μ = 3.8	μ = 6.5	μ = 4.0	μ = 2.2	6386
	σ = 0.5	σ = 7.5	σ = 3.3	σ = 1.2	
0.8%Fe-5%MM, T1	μ = 4.2	μ = 5.8	μ = 3.8	μ = 1.9	7227
	σ = 0.4	σ = 6.3	σ = 2.7	σ = 0.8	
0.8%Fe-0%MM, T3	μ = 4.2	μ = 7	μ = 4.6	μ = 2.2	5979
	σ = 0.7	σ = 7.7	σ = 4.0	σ = 1.3	
0.8%Fe-5%MM, T3	μ = 4.2 σ = 0.8	μ = 4.2	μ = 3.3	μ = 2.3	10812
		σ = 3.9	σ = 2.9	σ = 1.2	
1.2%Fe-0%MM, T1	μ = 3.5	μ = 5.4	μ = 4.0	μ = 2.2	7387
	σ = 0.6	σ = 7	σ = 3.4	σ = 1.0	
1.2%Fe-5%MM, T1	μ = 3.2	μ = 3.7	μ = 3.2	μ = 2.0	8983
	σ = 0.5	σ = 3.8	σ = 2.3	σ = 0.8	
1.2%Fe-0%MM, T3	μ = 4.3	μ = 5.2	μ = 4.0	μ = 2.2	8809
	σ = 0.7	σ = 6.5	σ = 3.3	σ = 1.2	
1.2%Fe-5%MM, T3	μ = 2.8	μ = 3.3	μ = 2.8	μ = 2.0	9694
	σ = 0.6	σ = 3.5	σ = 2.2	σ = 0.8	

Fig. 6. Precipitation of α-Fe in 0.8%Fe, 5%MM poured from:(a) 750 °C, (9b) 950 °C.

mechanism of the observed Si modification in this case is rather mechanically which is different than that reported for Sr modification [33, 34].

Fig. 10a and b illustrate the variation in the morphology of the eutectic silicon as a function of the pouring temperature (0.46%Fe-0% MM). Pouring from 750 °C resulted in long un-modified eutectic Si particles (black square) - black arrow point to formation of microporosity at the interception of the Si plaquettes. Casting the same alloy from 950 °C, Fig. 10b, reveals partial fragmentation of the Si plaquettes (black square) with disappearance of the microporosity due to high fluidity of the molten metal. In order to highlight the role of solidification rate and hence solidification time on the morphology and size of β-platelets, samples containing 1.2%Fe-0%MM, poured in metallic mold from 750 °C have been examined as shown in Fig. 11a revealing marked reduction in both size and density of the Fe-platelets. The decomposition of β-platelets through the rejection of Si into the surrounding matrix during solutionizing treatment is exhibited in Fig. 11b leading dissolution of most of β-phase particles as clearly demonstrated in Fig. 11c. It

should be emphasized here that solidification time in this case is about 80s-thermocoupled was placed near the gaged length.

Another variant of Fe-intermetallics is the formation of sludge depending on the process parameters (melt temperature and holding time) rather than the alloy chemical composition. In order to highlight the effect of the chemical composition on the sludge formation, Jorstad [35] and Groteke [36] proposed a Sludge Factor (SF) = (1 × wt. %Fe) + (2 × wt. %Mn) + (3 × wt. %Cr). To minimize the sludge formation, a small SF needs to be maintained. Fig. 11a illustrates the persistence of segregated platelets (see arrow) after solutionizing treatment (Fig. 11b) and the increase in their volume fraction with increasing the Fe content as the SF increase (Fig. 11c). From the fracture analysis of tensile tested samples examined by Bjurenstedt et al. [37], the authors concluded that that the mechanical properties were mainly governed by the Fe-rich particles, which were fracturing through cleavage as revealed in Fig. 11d of tensile sample was tested from same conditions of Fig. 11b.
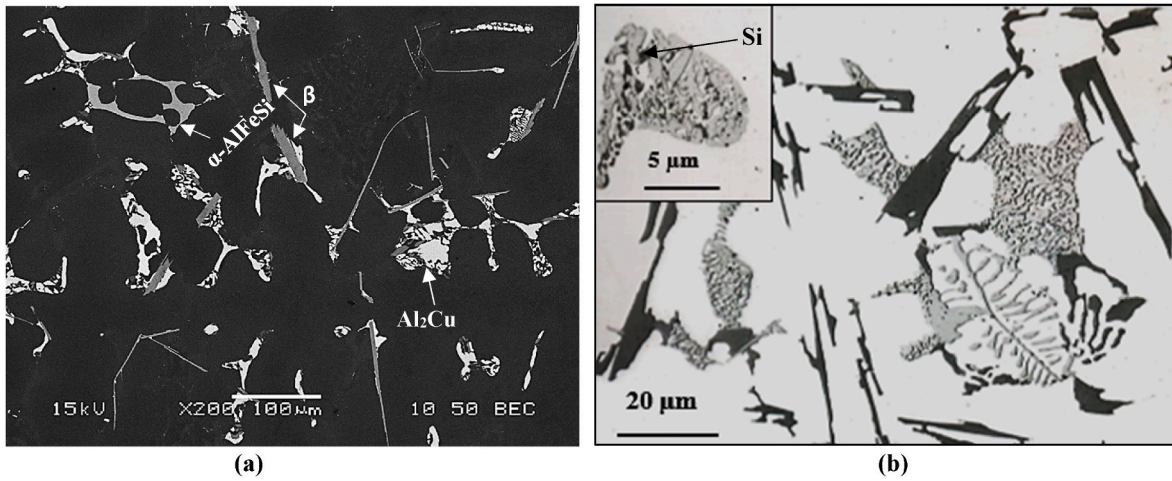
Fig. 7. Microstructure obtained from 0.46%Fe-0%MM in the as condition: (a) precipitation of Al2Cu on the long surfaces of β-platelets, (b) precipitation of Al2Cu on the edges of α-Fe.
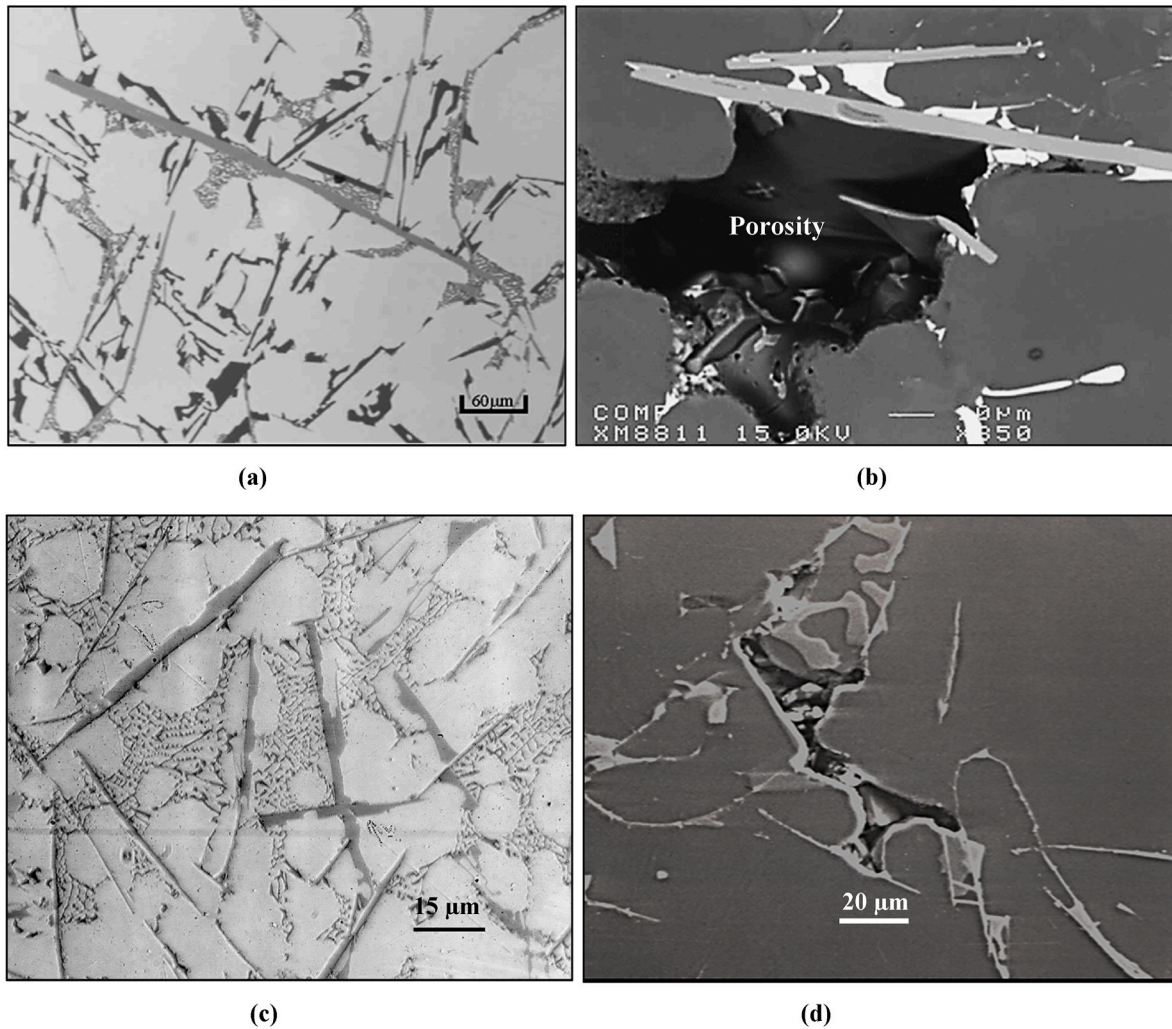

Fig. 8. Microstructure of 1.2%Fe-no Mischmetal: (a) optical micrograph, (b) backscattered electron image, (c) optical micrograph of samples poured from 950 °C, (d) example of porosity formation relation to Fe-intermetallics.

3.3. Tensile properties

For all alloys, the average surface area (in %) of the silicon phase and other phases, the length average, the density which represents the number of particles per mm^2 and the average particle length/width ratio were measured. According to Fig. 5, the 0.4% Fe base alloy cast at
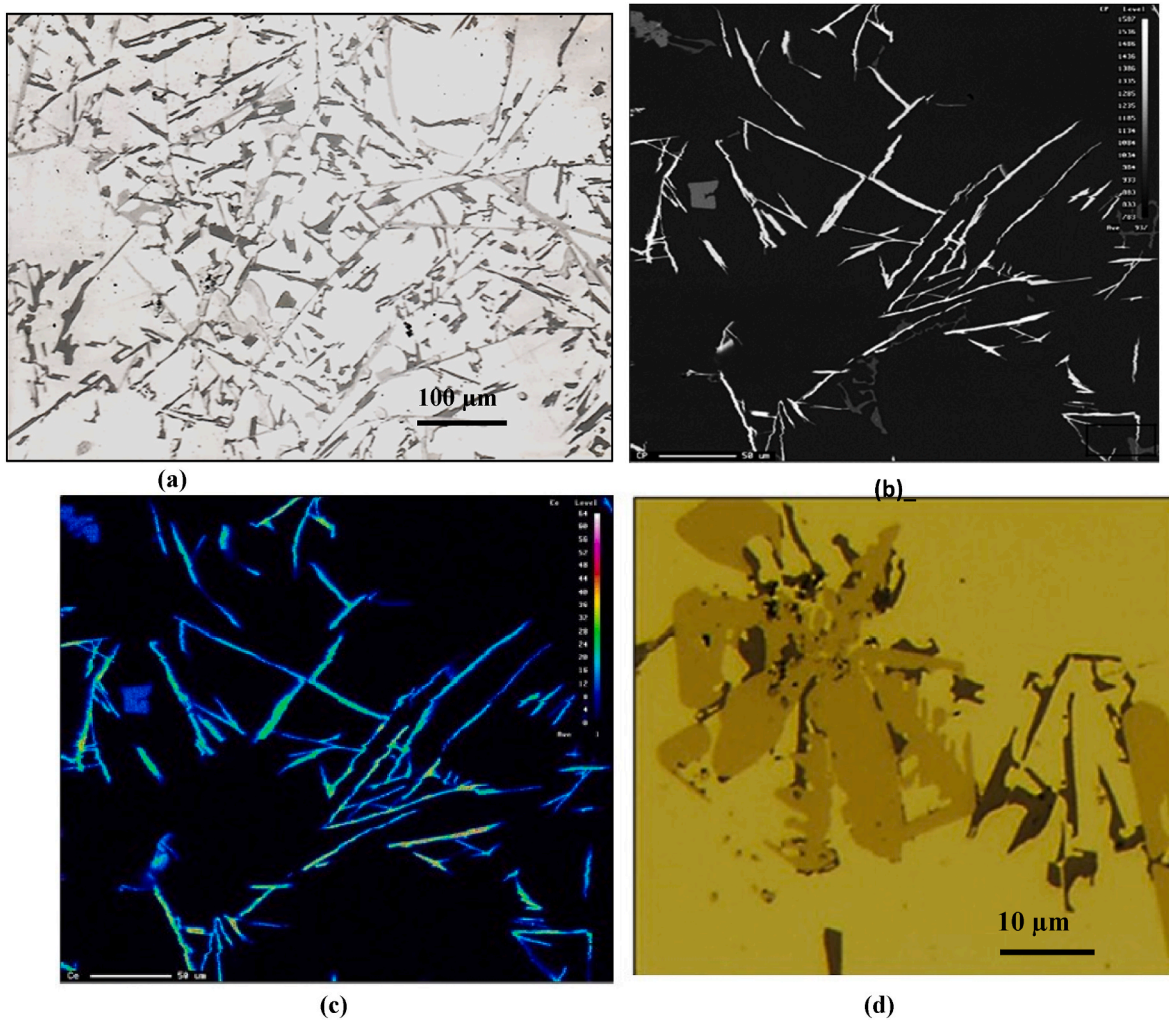
Fig. 9. Precipitation of RE based intermetallic in 0.46%Fe-5%MM: (a) optical microstructure, (b) backscattered electron image of (a), (c) Ce distribution in (b), (d) precipitation of eutectic Si particles on the surface of the existing RE phase particles.

Fig. 10. Morphology of eutic Si plaquettes in samples poured from:(a) 750 °C, (b) 950 °C.

temperature T1 of 750 °C, undergoes noticeable modifications at the level of the silicon phase (Table 6). This change manifests itself by fragmentation of the particles of silicon, also confirmed by Wang et al. [38], and by the increase their density (particles/mm2). Some results

obtained in present study confirm the effect of iron on the eutectic silicon phase. Indeed, in the base alloys with no mischmetal, it is noticed a marked increase in density eutectic silicon when the iron concentration is increased. This increase is of the order of 34% when the iron
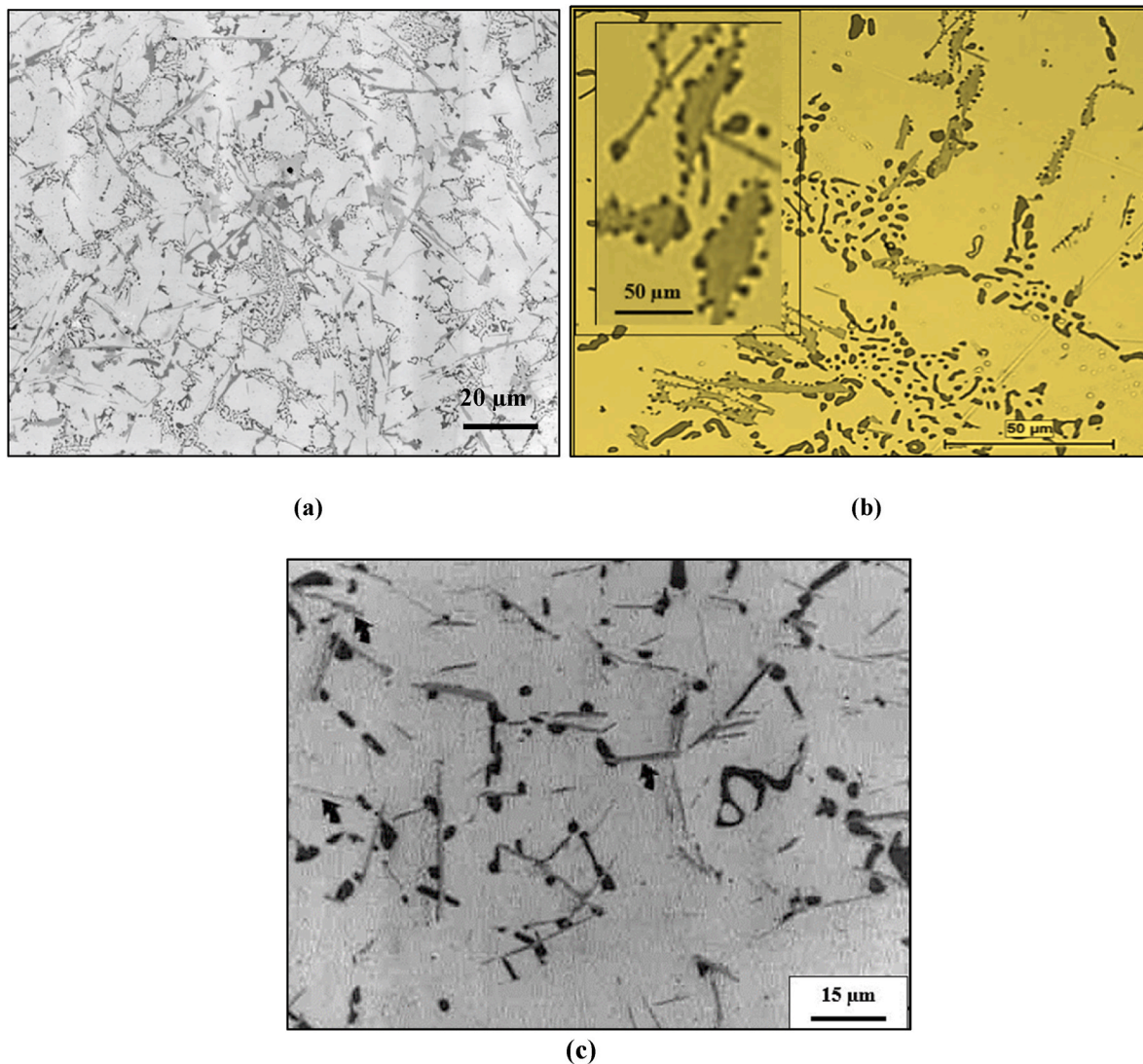
(a)

(b)

(c)

Fig. 11. Microstructure of a sample containing 1.2%Fe-0%MM cast in metallic mold from 750 °C: (a) as-cast, (b,c) after T6 treatment-note the remaining of β-platelets.

concentration increases from 0.4% to 1.2%. This is confirmed by the reduction in the surface area and length of each silicon particle, respectively 29% and 43.8%. There is decrease in the standard deviation showing that the effect of iron on the eutectic silicon phase affects more particles to 1.2% iron than 0.4%.

The morphological modification of the eutectic silicon phase by mischmetal is compared with that obtained by strontium in terms of microstructure mechanical properties and behavior. The conventional yield strength tensile strength percent elongation and hardness (under T6 conditions) in the alloy Al–7%Si-0.3%Mg increases by 20% when the amount of mischmetal added does not exceed 1%. The combination of grain refinement (reduction of interdendritic space) modification of eutectic silicon and formation of constituents such as AlCe and non-stoichiometric constituents between Al and Si. Mg, Fe, Ce and La. improve the mechanical properties of the alloy. Additions of mischmetal greater than 1% reduce the yield strength, the resistance to tensile strength and elongation percent while hardness increases [39]. The gradual increase in hardness beyond 2% can be explained by the formation of fine particles of intermetallic compounds.

The increase in the yield strength can be attributed in part to the change in the shape of the particles and the strengthening effect produced by the fine dispersion of hard intermetallic compounds such as Al_4Ce and Al_4La [40,41]. For aluminium at 99.5% purity, Elgallad et al.

[42] mentions that there is an improvement in the percentage with optimal additions of 0.3% of La and 0.2% of Nd; in addition, there is an improvement in machinability for optimal additions of 0.5% Ce. 0.05% La and 0.1% Nd. For the alloy 195 used by Sharan (13), an increase in the percentage of elongation is reported with additions of 1.5% of Ce. 0.3% of La and 0.1% of Nd. In addition. the hardness has undergone a very significant increase with additions of 0.3% La, 0.1% Nd and 1% mischmetal. Machinability has undergone a strong improvement with optimal additions of 0.1 % of La and 2% of mischmetal.

Moussavi et al. [43] observed that the hardness of alloys treated with T6 heat treatment does not change (100 VHN). The hardness is independent of the iron concentration and the superheating temperature. In the case of die casts, the AlFeSi constituents formed in Chinese script do not present themselves in a particular form as seen in sand mold castings although they can be distinguished from the morphology of the β phase and straight lines. The tensile strength for all iron levels was altered by the increase in the superheat temperature from 750 °C to 850 °C while the ductility was greatly increased. The surface area of the tensile bars for alloys with 0.5% Fe was found to be equal to that for alloys with 0.1% Fe.

Fig. 13 summarizes the mechanical tensile properties of the alloys studied in this project, whereas Fig. 14 depicts the contribution of added elements and superheating temperature to the tensile properties of the
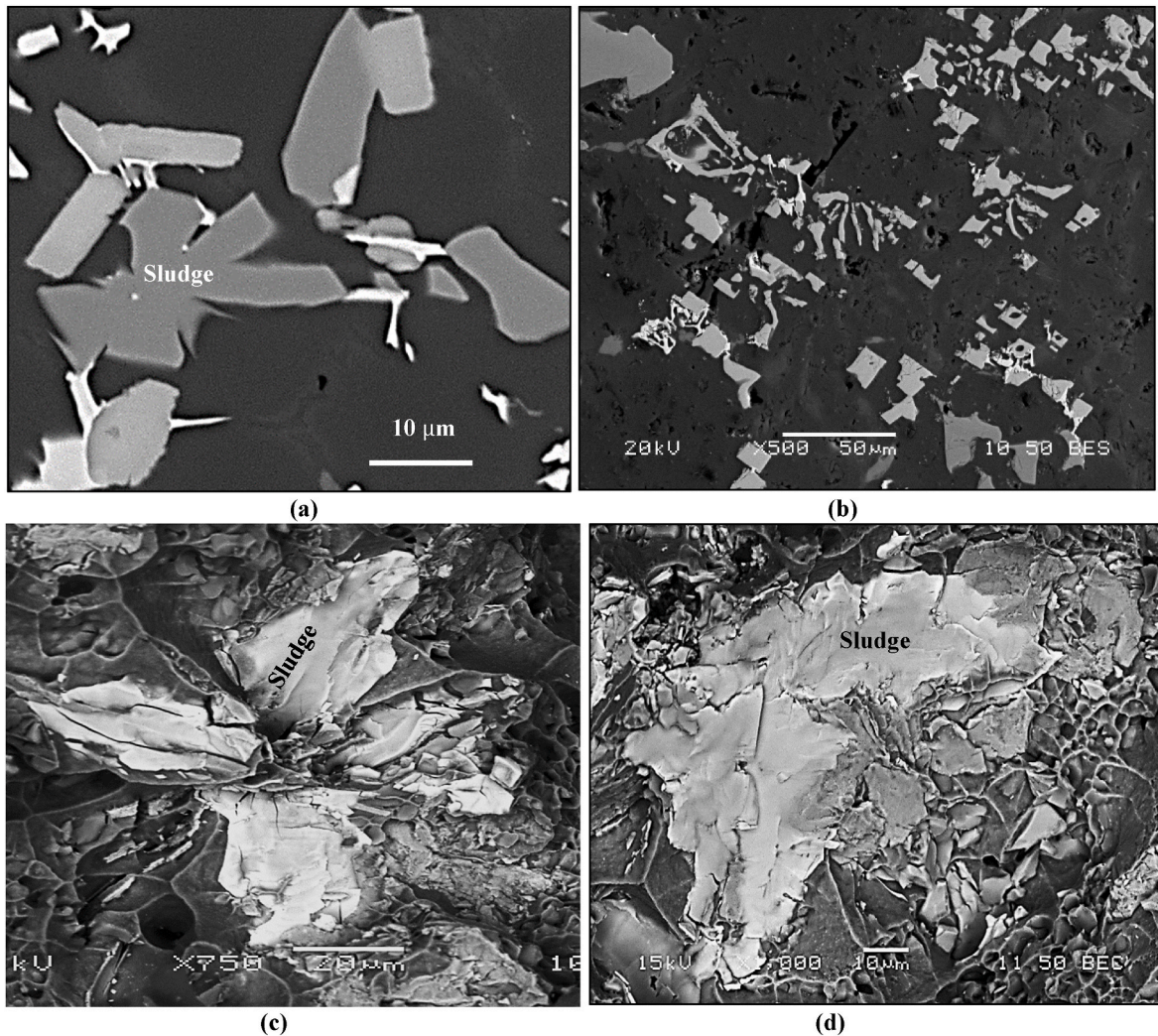
Fig. 12. (a) sludge in 0.46%Fe sample, (b) sludge in 1.2% Fe sample, (c) fracture of a sludge particle in (b), (d) cleavage fracture of a sludge particle in 1.2% alloy-no MM was added.

base alloy (method of calculation is shown in Appendix A). The parameters measured are the conventional elastic limit, the tensile strength and the elongation percent. The metallographic analysis of the silicon phase after T6 treatment concerns only the two extreme concentrations of mischmetal; 0% and 5% by weight as illustrated in Table 2. In the case of 0.4% Fe alloys, the elongation percent and tensile strength decrease as the mischmetal concentration and superheat temperature increase, as shown in Figs. 12 and 13. This reduction is maximum with 5% mischmetal for the superheating temperature of 950 °C and is evaluated at 80% in the case of elongation percent and 43% in the case of tensile strength.

The harmful effects of iron result in a degradation of the mechanical tensile properties of aluminum-silicon alloys [44,45]. In addition, the new phase of the misch-metal in the shape of needles will contribute to blocking the liquid metal and forming porosities which will degrade the ductility of these alloys. The mechanical properties of 0.8% iron alloys deteriorate when the concentration of mischmetal and the superheat temperature increase, although the phase of silicon undergoes significant changes as shown in Table 6. This deterioration can be attributed to the β-phase and the new phase of the needle-shaped mischmetal. In fact, it reaches a maximum value of 71% in the case of elongation percent and 32% in the case of tensile strength at 5% in mischmetal as shown in Figs. 13a and 14a.

The yield strength of conventional strength is slightly reduced in the

case of alloys with 1%, 3% and 5% mischmetal cast at 750 °C. There is a slight decrease for the alloy containing 5% mischmetal compared to the alloy containing 3%. This reduction reaches a maximum value of 27% in the alloy containing 5% mischmetal compared to the base alloy (Figs. 13b & 14b). In addition, the eutectic silicon phase does not undergo any major change in density. For the base alloys 0.4%Fe- 0% mischmetal, there was no improvement in mechanical properties with the increase in superheating temperature, contrary to what some researchers obtained for other Al–Si alloys.

In alloys with a high iron concentration (1.2% Fe), it was found that the length of the phase β and of the mischmetal does not increase but decreases slightly compared to alloys at 0.4%Fe and 0.8%Fe when the concentration of mischmetal increases to 5% and when the superheating temperature is 950 °C. This explains the relative increase in elongation percent for the 1.2%Fe-5%mischemtal alloy cast at 750 °C and 950 °C as illustrated in Figs. 12c and 13c. This increase is relative and not absolute since the percentage length of these alloys is always lower than that of alloys containing 0.4% iron. Tensile strength and yield strength degrade with mischmetal but improve slightly with overheating; only the 1.2% Fe-0%mischmetal alloy sees its yield strength decrease once superheated to 950 °C (Figs. 13c &14c). An improvement in hardness can be expected for the latter alloys.
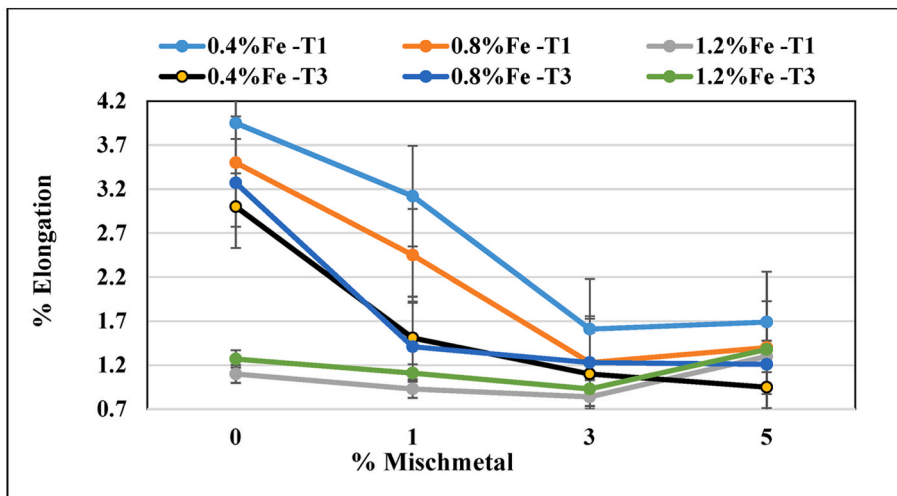
The quality of aluminum alloy castings may be defined using numerical values, which correlate their mechanical properties. Drouzy
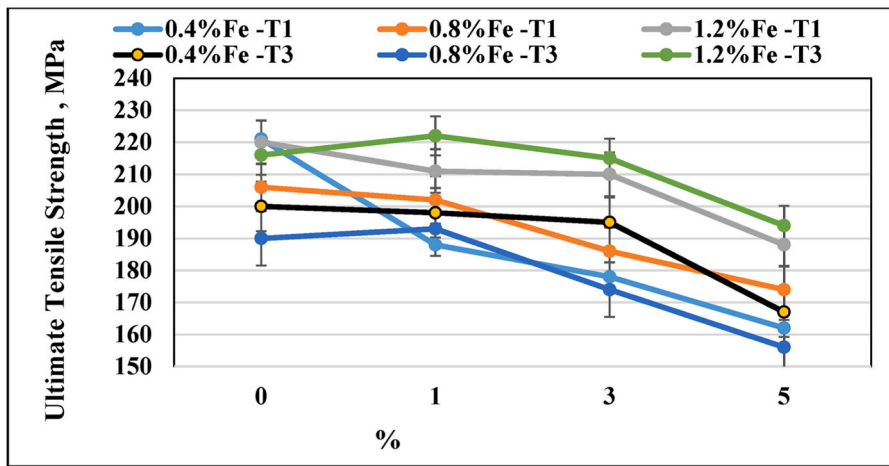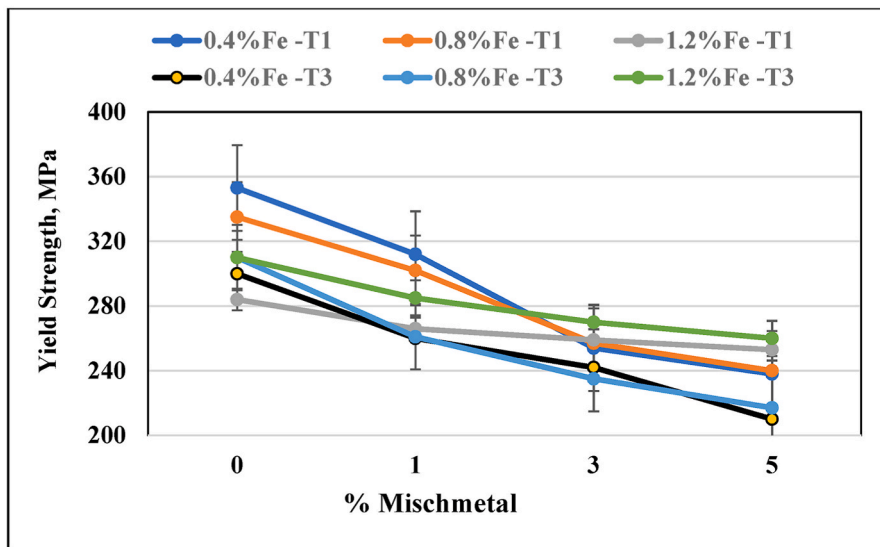
Fig. 13. Effect of additives and superheating on the alloys tensile properties: (a) UTS, (b) YS, (c) %El.

et al. [46,47] first proposed these numerical values in 1980 and termed them quality indices; these may be represented by the following equation:

$$Q = \sigma_{uts} + d \log \left(E_f \right) \qquad \text{Equation 1}$$

where Q is the quality index in *MPa*; σ_{uts} refers to the ultimate tensile
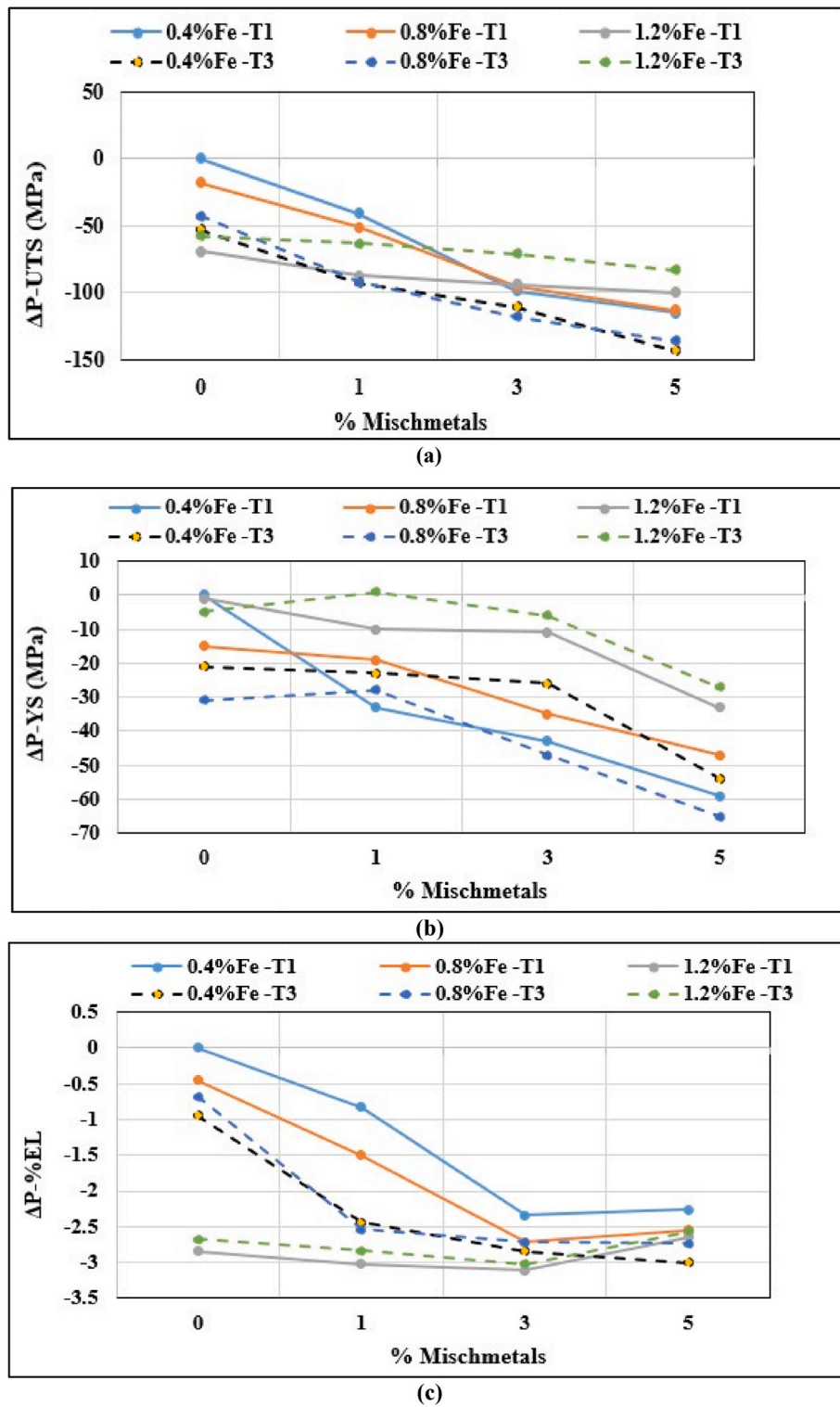
Fig. 14. Contribution of additives to the tensile properties of base alloy (0.46%Fe-0%MM):
(a) UTS, (b) Ys, (c) %El.

strength in *MPa*; E_f refers to the percentage elongation to fracture; and *d* is a material constant equal to 150 MPa for Al–7Si–Mg alloys. The probable yield strength ($\sigma_{P(YS)}$) for the same alloy may be proposed as:

Fig. 15 displays the Q-values of the alloys containing 0.46%, 0.84%, 1.2%Fe with 0% or 5% MM poured from 750 °C (T1) or after superheating at 950 °C (T3). As can be observed, for alloys with no RE, the Q-levels span over about 170 MPa. The effect of increasing the iron content resulted in decreasing the UTS level from 353 MPa (0.46%Fe) to 284

MPa (1.2%Fe) due to the increased volume fraction of β-platelets coupled with the increase in their platelets size. The effect of increasing the superheating temperature from 750 C to 950 C caused a slight decrease in the both UTS and %El of the base alloy (−50 MPa and −1% EL) which can be accounted for oxidation of the melt at such a temperature where it is difficult to degas the molten bath using a graphite impeller. Major reduction in the Q-levels occurred when 5% of mischmetal was added where all parameters (UTS, %El, and Q) were
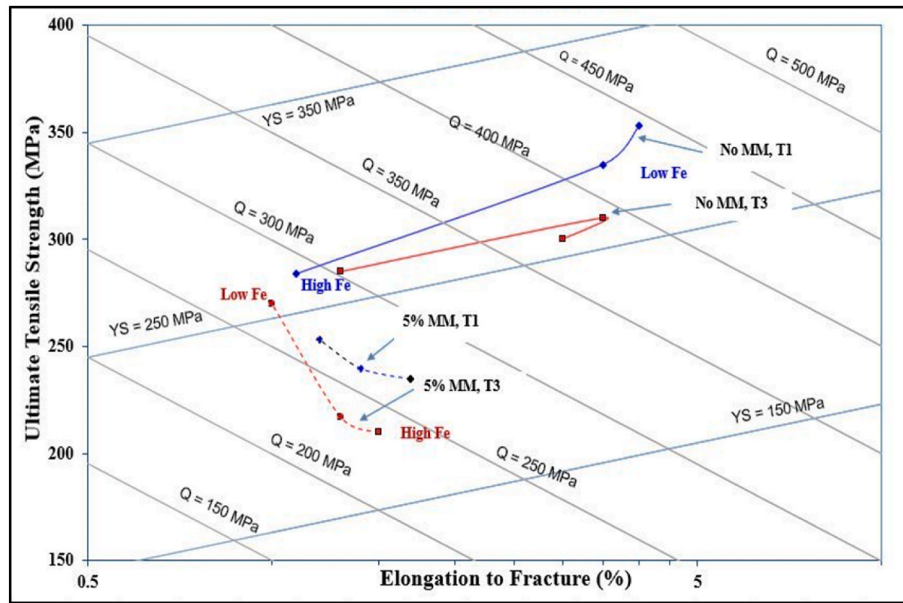
Fig. 15. Effect of additives on the Q-level of the present alloys.

significantly dropped with the presence of a marked amount of RE-based insoluble intermetallics [48].

$$\sigma_{P(YS)} = a\,\sigma_{UTS} - b \log\left(E_f\right) + c \qquad \text{Equation 2}$$

where the coefficients a, b, and c for Al–7Si–Mg alloys were determined as 1, 60, and −13, respectively, where the constants b and c are expressed in units of MPa.

4. Conclusions

Based on the resulted presented in this work, the following conclusions can be drawn:

1. In all 319 alloys no undercooling was observed during the Al–Si eutectic reaction Out of equilibrium the Al–Si T_E first eutectic reaction temperature of the base alloy 0.4%-Fe decreases once superheated to T = 950 °C, while the density of the silicon decreases. Probably the time of the moment of the reaction prevailed over the decrease in the temperature of the eutectic, given that in this case, this reaction takes place produced a second later.
2. The morphological modification of the silicon phase by iron in base alloys not containing mischmetal was confirmed. This change is noticeable when the iron content increases from 0.4 to 1.2% by weight. It corresponds to a 34% decrease in the average surface area of the phase particles. However, this process is not accompanied by an improvement in the mechanical characteristics of these alloys.
3. The addition of mischmetal produces a change in the morphology of the eutectic silicon phase that is greater than the increase in the superheat temperature.

4. The addition of iron combined with the addition of mischmetal and superheating results in a 76% increase in the particle density of the silicon phase compared to the base alloy 0.4%Fe- 0%MM- T1, and a 67% refinement in the particles average surface area.
5. The β-AlFeSi and α-AlFeSi intermetallic particles as well as mischmetal-bound intermetallics are insoluble i.e., they remain in the microstructure, even after the T6 heat treatment.
6. The new phase related to the mischmetal precipitates in the form of thin curved platelets, blocking the movement of liquid metal during casting and leading to porosity formation, which eventually will result in the degradation of the mechanical properties of these alloys.
7. The mechanical properties of the A319 alloys and in particular the decrease in elongation percent in the case of alloys with 0.8% Fe and 5% mischmetal. However, these properties are improved with increasing the iron content to ~1.2%.
8. The decrease in the length of the β-platelets is the main cause in controlling the alloy tensile properties. The relative improvement in the percentage of elongation to rupture in the case of high-iron alloys has opened up a new avenue in the recycling industry. At present, this process is only possible with alloys containing 5% mischmetal and cast from the temperature 950 °C.
9. Addition of mischmetal would lead to precipitation of massive volume fraction of RE platelets, acting as suitable nucleation sites for the precipitation of the eutectic Si particles leading to a major *refinement* of their size, which is different than the *modification* by Sr.

Declarations of interest

There is no conflict of interest between the authors.

Appendix A. Calculation of ΔP

The comparison system used consists of observing the difference between the properties of an alloy and those of alloy. The values were calculated as follows:

UTS(x) − UTS(I) = ΔUTS(x)

In this formula, UTS(x) represents the ultimate limit of the alloy with one or more new elements added; UTS(I) represents the ultimate limit of alloy I and ΔLUx is the difference between the two, which will serve as a comparison tool. The same calculation was also applied for the elastic limit (YS) and for the percentage of deformation (%El). According to this calculation, a result with a positive value indicates an increase in properties, while a

negative value means there has been a decrease. The main trend that emerges when analyzing the results obtained for the alloys as-cast is that there is an increase in the ultimate tensile limit and the elastic limit when the different elements are added. On the other hand, this results in a more or less marked reduction in the percentage of deformation.

References

[1] Khettabi R, Songmene V, Zaghbani I, Masounave J. Modeling of fine and ultrafine particle emission during orthogonal cutting. Journal of Materials Engineering and Performance. JMEPEG 2010;19:776–89.

[2] Kishor M, Chopra K, Ayyagari KPR. Tackling Fe-rich intermetallics in Al-Si alloy: a critical review. Trans Indian Inst Met 2024;77:3031–6. https://doi.org/10.1007/s12666-023-03205-8.

[3] Mathew J, Remy G, Williams MA, et al. Effect of Fe intermetallics on microstructure and properties of Al-7Si alloys. JOM 2019;71:4362–9. https://doi.org/10.1007/s11837-019-03444-5.

[4] Khan MH, Das A, Li Z, Kotadia HR. Effects of Fe, Mn, chemical grain refinement and cooling rate on the evolution of Fe intermetallics in a model 6082 Al-alloy. Intermetallics 2021;132:107132.

[5] Mohamed AMA, Samuel E, Zedan Y, Samuel AM, Doty HW, Samuel FH. Intermetallics Formation during solidification of Al-Si-Cu-Mg cast alloys. Materials 2022;15:1335. https://doi.org/10.3390/ma15041335.

[6] Samuel AM, Zedan Y, Doty HW, Songmene V, Samuel FH. A review study on the main sources of porosity in Al-Si cast alloys. Adv Mater Sci Eng 2021;2021:1921603.

[7] Zhao Y, Song D, Wang H, Jia Y, Lin B, Tang Y, Tang Y, Shu D, Sun Z, Fu Y, Zhang W. Revealing the influence of Fe on Fe-rich phases formation and mechanical properties of cast Al-Mg-Mn-Fe alloys. J Alloys Compd 2022;901:163666.

[8] Liu C, Jiao X, Nishat H, Akhtar S, Wiesner S, Guo Z, Xiong S. Characteristics of Fe-rich intermetallics compounds and their influence on the cracking behavior of a newly developed high-pressure die cast Al-4Mg-2Fe alloy. J. Alloy. Compd. 2021;854. https://doi.org/10.1016/j.jallcom.2020.157121. Article 157121.

[9] Zhao Y, Zhang W, Song D, Lin B, Shen F, Zheng D, Xie C, Sun Z, Fu Y, Li R. Nucleation and growth of Fe-rich phases in Al-5Ti-1B modified Al-Fe alloys investigated using synchrotron X-ray imaging and electron microscopy. J Mater Sci Technol 2021;80:84–99. https://doi.org/10.1016/j.jmst.2020.12.011.

[10] Li Z, Samuel AM, Samuel FH, Ravindran C, Valtierra S, Doty HW. Einflußfaktoren auf die Auflösung der CuAl2 -Phase in der Legierung 319. Giesserei-Praxis 2004;3:99–108.

[11] Mahta M, et al. Overview of B-Al5FeSi phase in Al-Si alloys. Materials Science Research Trends 2008:251–72.

[12] Gorny A, Manickaraj J, Cai Z, Shankar S. Evolution of Fe based intermetallic phases in Al-Si hypoeutectic casting alloys: influence of the Si and Fe concentrations, and solidification rate. J Alloys Compd 2013;577:103–24.

[13] Rivlin V, Raynor GV. Critical evaluation of constitution of aluminium–iron–silicon system. Int Met Rev 1981;3:133–52.

[14] Ahmad R, Marshall RI. Effect of superheating on iron-rich plate-type compounds in Aluminium-Silicon alloys. Int J Cast Metals Res 2003;15:497–504. https://doi.org/10.1080/13640461.2003.11819535. 2003.

[15] Wang Q, Geng H, Zhang S, et al. Effects of melt thermal-rate treatment on Fe-containing phases in hypereutectic Al-Si alloy. Metall Mater Trans A 2014;45:1621–30. https://doi.org/10.1007/s11661-013-2081-4.

[16] Narayanan LA, Samuel FH, Gruzleski JE. Crystallization behavior of iron-containing intermetallic compounds in 319 aluminum alloy. Metall Mater Trans 1994;25(8):1761–73.

[17] Mahmoud MG, Zedan Y, Samuel AM, et al. The use of rare earth metals in Al–Si–Cu casting alloys. Inter Metalcast 2022;16:535–52. https://doi.org/10.1007/s40962-021-00640-5.

[18] Nogita K, et al. The role of trace element segregation in the eutectic modification of hypoeutectic Al–Si alloys. J Alloys Compd 2010;489:415–20.

[19] Colombo M, Gariboldi E, Morri A. Er addition to Al-Si-Mg-based casting alloy: effects on microstructure, room and high temperature mechanical properties. J Alloys Compd 2017;708:1234–44.

[20] Emadi D, Rao AKP, Mahfoud M. Influence of scandium on the microstructure and mechanical properties of A319 alloy. Mater. Sci. Eng. A Struct. Mater. Prop. Microstruct. Process. 2010;527:6123–32.

[21] El Sebaie O, et al. The effects of mischmetal, cooling rate and heat treatment on the hardness of A319.1, A356.2 and A413.1 Al–Si casting alloys. Mater. Sci. Eng. A. 2008;486:241–52.

[22] Mousavi GS, Emamy M, Rassizadehghani J. The effect of mischmetal and heat treatment on the microstructure and tensile properties of A357 Al–Si casting alloy. Mater. Sci. Eng. A Struct. Mater. Prop. Microstruct. Process. 2012;556:573–81.

[23] Colombo M, Gariboldi E, Morri A. Er addition to Al-Si-Mg-based casting alloy: effects on microstructure, room and high temperature mechanical properties. J Alloys Compd 2017;708:1234–44.

[24] Colombo M, Albu M, Gariboldi E, Hofer F. Microstructural changes induced by Er and Zr additions to A356 alloy investigated by thermal analyses and STEM observations. Mater Char 2020;161:110117.

[25] Barkov RY, Prosviryakov AS, Khomutov MG, et al. Effect of the Zr and Er content on the structure and properties of the Al–5Si–1.3Cu–0.5Mg alloy. Phys Met Metallogr 2021;122:614–20. https://doi.org/10.1134/S0031918X21060028.

[26] Barkov RY, Mochugovskiy AG, Khomutov MG, et al. Effect of Zr and Er small additives on the phase composition and mechanical properties of Al–5Si–1.3Cu–0.5Mg alloy. Phys Met Metallogr 2021;122:161–8. https://doi.org/10.1134/S0031918X21020022.

[27] Mao F, Qiao Y, Zhang P, et al. Modification mechanism of rare earth Eu on eutectic Si in Al-Si alloy. Inter Metalcast 2022;16:634–45. https://doi.org/10.1007/s40962-021-00626-3.

[28] Yıldırım M, Özyürek D. The effects of Mg amount on the microstructure and mechanical properties of Al–Si–Mg alloys. Mater Des 2013;51:767–74.

[29] Zhu M, Jian Z, Yang G, Zhou Y. Effect of T6 heat treatment on the microstructure, tensile properties sand fracture behavior of the modified A356 alloys. Mater Des 2012;36:243–9.

[30] Haghdadi N, Zarei-Hanzaki A, Roostaei AA, Hemmati AR. Evaluating the mechanical properties of a thermo mechanically processed unmodified A356 Al alloy employing shear punch testing method. Mater Des 2013;43:419–25.

[31] Narayanan LA, Samuel FH, Gruzleski JE. Dissolution of iron intermetallics in Al-Si Alloys through nonequilibrium heat treatment. Metall Mater Trans 1995;26:2161–74.

[32] Musmar S, Mucciardi FA, Gruzleski JE, Samuel FH. A novel in-situ thermal analysis technique for aluminum alloys 356, 319, Al-xSi, Al-Si-Cu-xMg and 6063 experimental study. In: Transactions of the American foundry society: volume 115; 111th annual metalcasting congress. Houston, Tex.]: American Foundry Society; May . 2007.

[33] De Giovanni M, Kaduk JA, Srirangam P. Modification of Al-Si alloys by Ce or Ce with Sr. JOM 2019;71:426–34. https://doi.org/10.1007/s11837-018-3192-6.

[34] Campbell J, Tiryakioğlu M. Review of effect of P and Sr on modification and porosity development in Al–Si alloys. Mater Sci Technol 2010;26(3):262–8. https://doi.org/10.1179/174328409X425227.

[35] Jorstad JL. Die casting engineer, vol. 30; 1986. p. 1–6.

[36] Groteke DE. Die casting engineer 1985;5(29):16–24.

[37] Bjurenstedt A, Seifeddine S, Jarfors AEW. The effects of Fe-particles on the tensile properties of Al-Si-Cu alloys. Metals 2016;6:314. https://doi.org/10.3390/met6120314.

[38] Li Q, Wang JS, Liu XX, Wang B. Minimizing detrimental impacts of β-Fe in Al–Mg–Si alloy by combining thermal and compression processes. Mater Char 2023;198:112752–68.

[39] Sharon R, Anantharaman TR. Modification of aluminum-silicon alloys by mischmetal additions. Curr Sci 1967;21:568–70.

[40] Nogita K, McDonald SD, Dahle AK. Eutectic modification of Al-Si alloys with rare earth metals. Mater Trans 2004;45(2):323–6.

[41] Mazahery A, Shabani MO. Modification mechanism and microstructural characteristics of eutectic Si in casting Al-Si alloys: a review on experimental and numerical studies. JOM 2014;66:726–38. https://doi.org/10.1007/s11837-014-0968-1.

[42] Elgallad EM, et al. Effects of La and Ce addition on the modification of Al-Si based alloys. Adv Mater Sci Eng 2016;2016(1):5027243.

[43] Mousavi GS, Emamyn M, Rassizadehghani J. The effect of mischmetal and heat treatment on the microstructure and tensile properties of A357 Al–Si casting alloy. Mater. Sci. Eng. A. 2012;556:573–81.

[44] Taylor John A. Iron-containing intermetallic phases in Al-Si based casting alloys. Procedia Materials Science 2012;1:19–33.

[45] Koech Pius K. A study on the effects of iron on microstructure and mechanical properties of Aluminium-Silicon alloys. Kenya: Diss. University of Nairobi; 2012.

[46] Drouzy M, Jacob S, Richard M. Interpretation of tensile results by means of quality index and probable yield strength. AFS Int. Cast Met. J. 1980;5:43–50.

[47] Jacob S. Quality index in predicting of properties of aluminum castings—a review. AFS Trans. 2000;108:811–8.

[48] Mahmoud MG, Samuel AM, Doty HW, Valtierra S, Samuel F, H. Effect of solidification rate and rare earth metal addition on the microstructural characteristics and porosity formation in A356 alloy. Adv Mater Sci Eng 2017;2017:1–19.